

Material Characterization Approach for Modeling High-Strength Concrete after Cooling from Elevated Temperatures

Arano, Assis; Colombo, Matteo; Martinelli, Paolo; Øverli, Jan Arve; Hendriks, Max A.N.; Kanstad, Terje; Di Prisco, Marco

DOI

[10.1061/\(ASCE\)MT.1943-5533.0003694](https://doi.org/10.1061/(ASCE)MT.1943-5533.0003694)

Publication date

2021

Document Version

Final published version

Published in

Journal of Materials in Civil Engineering

Citation (APA)

Arano, A., Colombo, M., Martinelli, P., Øverli, J. A., Hendriks, M. A. N., Kanstad, T., & Di Prisco, M. (2021). Material Characterization Approach for Modeling High-Strength Concrete after Cooling from Elevated Temperatures. *Journal of Materials in Civil Engineering*, 33(5), 04021086-1 - 04021086-17. Article 04021086. [https://doi.org/10.1061/\(ASCE\)MT.1943-5533.0003694](https://doi.org/10.1061/(ASCE)MT.1943-5533.0003694)

Important note

To cite this publication, please use the final published version (if applicable).
Please check the document version above.

Copyright

Other than for strictly personal use, it is not permitted to download, forward or distribute the text or part of it, without the consent of the author(s) and/or copyright holder(s), unless the work is under an open content license such as Creative Commons.

Takedown policy

Please contact us and provide details if you believe this document breaches copyrights.
We will remove access to the work immediately and investigate your claim.

Green Open Access added to TU Delft Institutional Repository

'You share, we take care!' - Taverne project

<https://www.openaccess.nl/en/you-share-we-take-care>

Otherwise as indicated in the copyright section: the publisher is the copyright holder of this work and the author uses the Dutch legislation to make this work public.



Material Characterization Approach for Modeling High-Strength Concrete after Cooling from Elevated Temperatures

Assis Arano¹; Matteo Colombo²; Paolo Martinelli³; Jan Arve Øverli⁴; Max A. N. Hendriks⁵; Terje Kanstad⁶; and Marco di Prisco⁷

Abstract: Advanced numerical modeling of high-strength concrete ($f_c > 60$ MPa) structures designed to withstand severe thermal conditions requires detailed and reliable information on the mechanical properties of the material exposed to elevated temperatures. The only uniaxial compressive strength variation with temperature is not enough to satisfy the large number of parameters often required by advanced nonlinear constitutive models. For this reason, a complete experimental investigation is required. The paper takes a commonly used high-strength concrete ($f_c = 73$ MPa) as an example to describe a comprehensive experimental approach instrumental to the parameter definition and calibration of common constitutive models for concrete. The present study not only studied the overall compressive and tensile behavior of the case study material, but also investigated the effect of elevated temperatures on the specific fracture energy and the evolution of internal damage, in residual conditions after a single thermal cycle at 200°C, 400°C, and 600°C. DOI: [10.1061/\(ASCE\)MT.1943-5533.0003694](https://doi.org/10.1061/(ASCE)MT.1943-5533.0003694). © 2021 American Society of Civil Engineers.

Author keywords: Concrete mechanical properties; Thermal exposure; Residual conditions; Internal damage evolution; Fracture energy; Uniaxial tensile tests.

Introduction

Fires in European tunnels [e.g., Mont Blanc (France/Italy) 1999 or Tauern (Austria) 1999] have clearly shown the risks and consequences of high thermal loads on reinforced concrete structures. Although concrete is generally believed to be an excellent fire-proofing material, many studies have shown extensive damage or even catastrophic failure at high temperatures (Phan and Carino 2001). All these catastrophic events highlight the need of reliable modeling and design approaches able not only to predict service

condition but also to provide accurate prediction of tunnel structural behavior when exceptional conditions are taken into account.

Basic precondition of a reliable model is, of course, a proper definition of the material properties. As concrete is exposed to elevated temperatures, its mechanical properties, such as strength in both compression and tension and its stiffness, are adversely affected, to the detriment of both structural safety and durability. Comprehensive research has been carried out in recent decades to test normal-strength concrete (NSC) subjected to elevated temperatures (Abrams 1971; Anderberg and Thelandersson 1976; Felicetti and Gambarova 1998; Hager and Pimienta 2004; Janotka and Bágel 2002; Khaliq and Kodur 2012; Khoury 1992; Khoury et al. 1999; Naus 2006; Phan and Carino 2001; Sancak et al. 2008; Schneider 1985). Some of these studies are also referred to in the codes [Eurocode 2 (CEN 2004b, 2019); Eurocode 4 (CEN 2005)]. In addition, more advanced techniques based on numerical and artificial intelligence (AI) approaches have been used in the recent years to further explore the material behavior at elevated temperatures (Bingöl et al. 2013; Lam and Fang 2014; Nechnech et al. 2002; Neuenschwander et al. 2016; Tanyildizi 2009).

High-strength concrete (HSC) offers various benefits derived from its greater stiffness and strength (60–120 MPa), and its use has become increasingly popular. However, HSCs are more sensitive than NSCs to high temperatures because of their reduced porosity, which favors steam pressure build-up and increases their susceptibility to explosive spalling. To avoid this effect, one commonly adopted solution is to add polypropylene (PP) microfibers (Hager and Mróz 2019; Kalifa et al. 2001). The research studies available on HSC subjected to elevated temperatures indicate that results strongly depend on the type of aggregate, heating rate, and content of PP fibers [fib 38 (fib 2007); Siddique and Noumowe 2010]. The large variation in the findings, therefore, makes it challenging to obtain accurate material behavior curves. This motivates further investigation.

¹Ph.D. Candidate, Dept. of Structural Engineering, Norwegian Univ. of Science and Technology, Trondheim 7491, Norway (corresponding author). Email: assis.arano@ntnu.no

²Associate Professor, Dept. of Civil and Environmental Engineering, Politecnico di Milano, Milan 20133, Italy. Email: matteo.colombo@polimi.it

³Assistant Professor, Dept. of Civil and Environmental Engineering, Politecnico di Milano, Milan 20133, Italy. Email: paolo.martinelli@polimi.it

⁴Professor, Dept. of Structural Engineering, Norwegian Univ. of Science and Technology, Trondheim 7491, Norway. ORCID: <https://orcid.org/0000-0002-3546-9058>. Email: jan.overli@ntnu.no

⁵Professor, Dept. of Structural Engineering, Norwegian Univ. of Science and Technology, Trondheim 7491, Norway; Associate Professor, Faculty of Civil Engineering and Geosciences, Delft Univ. of Technology, 2628 CN Delft, Netherlands. ORCID: <https://orcid.org/0000-0001-9507-3736>. Email: max.hendriks@ntnu.no

⁶Professor, Dept. of Structural Engineering, Norwegian Univ. of Science and Technology, Trondheim 7491, Norway. Email: terje.kanstad@ntnu.no

⁷Professor, Dept. of Civil and Environmental Engineering, Politecnico di Milano, Milan 20133, Italy. Email: marco.diprisco@polimi.it

Note. This manuscript was submitted on July 16, 2020; approved on September 28, 2020; published online on February 27, 2021. Discussion period open until July 27, 2021; separate discussions must be submitted for individual papers. This paper is part of the *Journal of Materials in Civil Engineering*, © ASCE, ISSN 0899-1561.

The use of HSC ($f_c = 73$ MPa) with PP fibers is also of great interest for the Norwegian Public Roads Administration's (NPRA) ferry-free coastal route E39 project. This project is aimed at establishing a coastal highway route without ferry connections. Due to durability problems of the Norwegian infrastructure mainly related to reinforcement corrosion, the NPRA decided in the 1990s to require water/binder ratio = 0.4 in all Norwegian bridge structures. From both a durability perspective, and for contractual issues, the requirement has been successful, and such concrete is commonly denoted as Norwegian Bridge Concrete (Osmolska et al. 2019). New large concrete structures, such as submerged floating tunnel (SFT), need to be built to cross the wide and deep fjords along the coast, and it is of interest to evaluate the combined action of fire and blast loads inside tunnels. The design and prediction of the behavior of large RC structures typically involve the use of advanced nonlinear numerical approaches. The knowledge of strength evolution is not enough for these kinds of models, which require a more complete knowledge of the material constitutive behavior and, in particular, the definition of the whole uniaxial compressive and tensile behaviors also with the corresponding fracture energy.

When complex situations, like fire conditions, need to be investigated, the load path can also play a significant role; as an example, traditional ultimate limit state (ULS) loading condition can induce irreversible strain into the structure that can be later exposed to fire or vice versa. Under this point of view, damage evolution laws and their variation after high temperature exposure also become fundamental for an accurate prediction of the overall structural behavior. Nevertheless, there is no extended literature investigating these properties at high temperatures. Therefore, additional material tests studying the behavior of this type of HSC are vital for the design of the investigated structures for fire resistance.

Compressive strength, tensile strength, elastic modulus, and stress-strain response in compression are mechanical properties that are of primary interest in fire resistance design (e.g., Kodur 2014; Shah et al. 2019; Siddique and Noumowe 2010). If the compressive strength has been extensively investigated in the literature, conversely, splitting tensile strength, elastic modulus, and compressive stress-strain response have been less studied in the literature. Moreover, significantly less data or no data are available in the literature on direct tensile strength, tensile stress-strain response, tensile and compressive specific fracture energies, and internal damage at elevated temperatures.

The effect of the high temperature on the material properties can be evaluated in hot conditions, i.e., tested at maximum temperature, or in residual conditions, i.e., with a cooling phase after the heating cycle. In the literature, residual conditions are more commonly used due to additional challenges arising when performing experiments in hot conditions. Results from earlier studies (Felicetti et al. 2000; Felicetti and Gambarova 1999) show that tests in residual conditions are representative of the effect of high temperature on the material. It is also of great interest to model the postfire resistance and reliability of the structure, and therefore a residual material characterization is required. This further motivates the testing of specimens after cooling.

This study provides an example of a comprehensive approach for the mechanical material characterization aimed at an advanced numerical modeling. The experimental campaign investigates the effect of elevated temperatures in residual conditions on some necessary and less investigated mechanical properties of concrete, such as the uniaxial tensile strength and the specific compressive and tensile fracture energy. In addition, it presents the evolution of internal damage for both compressive and tensile behavior, which is obtained from the unloading-reloading cycles along the complete stress-strain curves. Moreover, this study provides an extended comparison with

previous research studies for well-investigated properties, such as compressive strength and the modulus of elasticity of concrete. Also, the reliability of existing damage evolution law at high temperature available in the literature is discussed.

The paper is aimed at presenting an experimental approach that is instrumental to assess all the main mechanical parameters that can be used for the modeling of concrete structures in case of fire. The approach aims at the identification not only of the most common parameters (e.g., compressive strength and elastic modulus) but also to all those parameters that are crucial when nonlinear analyses are adopted (e.g., fracture energy and damage evolution law). This study considers three high temperatures (200°C, 400°C, and 600°C), in addition to the reference room temperature (20°C). Additional partial results for 800°C are also presented. The paper mainly refers to residual condition (after cooling) because from an engineering point of view, the residual capacity of a structure after the fire exposure is the most interesting issue in order to assess the safety level of the structure after a critical event.

Mechanical Properties of Concrete at High Temperatures: Background

As already discussed, the aim of the present paper is to describe a complete mechanical characterization procedure for modeling concrete structures exposed to fire conditions. For this reason, the experimental tests should endeavor as much as possible to represent the constitutive behavior of the material, without introducing into the specimen any structural effect that, if not properly detected, could be confused with material properties (because the prediction of the structural effects is a task of the numerical models and not of the constitutive laws).

When testing materials at high temperature, a high temperature gradient can lead to additional thermal stresses and explosive spalling, which is not the aim of this study. The use of controlled heating and cooling rates can prevent these undesired events from occurring. Many research studies have examined the influence of different heating and cooling rates on concrete specimens. Thelandersson (1974) observed no effects using a heating rate of 2°C/min, while some specimens exploded when heating at 4°C–8°C/min. This agrees with data published by Khoury (1992), and Campbell-Allen and Desai (1967), who concluded that cooling rates lower than 2°C/min should be used to avoid undesired stresses. Research conducted by Felicetti and Gambarova (1998) showed that self-stresses are negligible using a heating and cooling rate of 0.2°C/min.

Residual mechanical properties of concrete are very dependent on the nature and mineralogical composition of the aggregate used (Xing et al. 2014). Eurocode 2 [EN 1992-1-2 (CEN 2004b)] shows that a siliceous aggregate concrete is more sensitive to high temperatures than a calcareous aggregate concrete, which is generally attributed to the higher thermal expansion of the former. Nevertheless, later studies by Xing et al. (2011) and Robert and Colina (2009) showed that concretes prepared with some siliceous aggregates can have better mechanical performance. Niry Razafinjato et al. (2016) recently concluded that the categorization of aggregates in the Eurocode is not accurate enough to precisely predict the high temperature behavior of concrete, suggesting that further studies should be carried out. However, this is not part of the aim of the present study.

In recent years, many authors have extensively investigated the influence of elevated temperatures on the compressive strength and modulus of elasticity. The most relevant studies for the present work are a selection of 14 publications (Bastami et al. 2011; Diederichs et al. 2009; Felicetti and Gambarova 1998;

Hager and Pimienta 2004; Janotka and Bágel 2002; Khoury et al. 1999; Morita et al. 1992; Noumowe 2003, 2005; Noumowe et al. 1996; Phan and Carino 2001; Poon et al. 2001; Sancak et al. 2008; Sullivan and Sharshar 1992), which investigate the strength after cooling of concretes with similar strength to the one used in this study. Eight of these publications also examine the effect of temperature on the modulus of elasticity (Diederichs et al. 2009; Felicetti and Gambarova 1998; Hager and Pimienta 2004; Janotka and Bágel 2002; Khoury et al. 1999; Noumowe 2003, 2005; Phan and Carino 2001).

Most of these studies report a decreasing tendency in stiffness with increasing temperatures. Only a few studies reported an increase in strength for temperatures below 200°C (Janotka and Bágel 2002; Khoury et al. 1999; Morita et al. 1992). Results reported by Felicetti and Gambarova (1998) show the most pronounced reduction in compressive strength, with only a 10% remaining strength at 500°C. No other author reported this rapid decrease. Instead, an average of 20% of the total strength remained in most of the studies at 800°C. Phan and Carino (2001) were alone in reporting a plateau effect between 100°C and 300°C. There is considerable scatter in compressive strength results for elevated temperatures from the different studies, even between comparable initial strength concretes. Nevertheless, a similar coefficient of variation (COV) equal to 38%, 33%, and 31% at 400°C, 600°C, and 800°C, respectively, can be observed. A state-of-the-art study presented by RILEM (Pimienta et al. 2019) confirmed that this scatter is due to different concrete mixtures and testing conditions.

Naus (2006) conducted a literature review on the effect of elevated temperature on concrete materials and structures. He observed that the decrease of modulus of elasticity was more pronounced than the decrease in compressive strength. Moreover, he concluded that the strength of concrete before testing had little effect on percentage of strength retained at elevated temperature. Later, Kodur (2014) studied the effect of high temperature on compressive strength, modulus of elasticity, and stress-strain response, among other properties of HSC. A large variation of results was found between 200°C and 500°C. In addition, a few data points were reported for HSC for temperatures higher than 500°C. A more recent review by Shah et al. (2019) reported that stress-strain relation of HSC exposed to fire was not comprehensively reported in literature, remarking its value to properly model the fire behavior of HSC. They concluded that data available is insufficient considering the number of parameters that should be investigated.

The use of nondestructive techniques was shown to have great potential to quantify the deterioration of concrete after fire exposure. Recent studies by Matysik et al. (2018) and Varona et al. (2018) found that the evolution of the (dynamic) elastic modulus was consistent with the background and concluded that ultrasonic pulse velocity (UPV) is appropriate for studying its degradation at elevated temperatures. The test consists of sending a pulse of ultrasonic waves through the material and determining the traveling velocity. Higher velocities indicate better material quality. The expected velocity in a not damaged concrete is 4.5–5 km/s (Jain et al. 2013).

The published data available on uniaxial tensile tests of concrete are limited, probably because of the complexity of the test procedure. Furthermore, findings are often conflicting due to the different specimen shapes or boundary conditions. Table 1 lists previous research on uniaxial tensile tests, detailing the specimens, the concrete, and the boundary conditions (fixed or rotating end) used. In addition, it specifies whether the concrete was subjected to high temperature (residual or hot conditions) or ambient temperature.

Zheng et al. (2001) investigated the effect of the bonding between the specimen and the steel loading plates. They concluded that the most reliable method of applying uniaxial tension (without inducing secondary stresses) is to glue the plates to the ends of the specimen.

Table 1 shows that the influence of high temperatures on the uniaxial tensile strength of concrete was only examined by Felicetti and Gambarova (1999, 2000) and Lam and Fang (2014). Results reported by Lam and Fang (2014) are significantly lower than the other test results considered. This may be due to the very slender shape of the specimens tested. Moreover, their results show little influence of elevated temperatures on tensile strength for temperatures up to 500°C. These results disagree with Felicetti and Gambarova (1999), where three different HSCs were tested, and observed a large strength decrease to $0.30f_{ct,20}$ at 400°C. A RILEM state-of-the-art report (Pimienta et al. 2019) remarked on the need for a research program to investigate the effect of high temperatures on the tensile strength of HSC.

Testing materials using a displacement-controlled procedure makes it possible to obtain a complete stress-strain curve and thereby evaluate the specific fracture energy. This property is a fundamental material parameter required by most mathematical models based on concrete fracture mechanics, because it denotes the energy needed to propagate a crack. Felicetti and Gambarova (1999) studied the effect of high temperatures on specific tensile

Table 1. Previous research studies on uniaxial tensile tests

References	Specimens			Boundary conditions	Compressive strength (MPa)	Temperature (°C)
	Shape	Size (mm)	Notched/unnotched			
Zhen-Hai and Xiu-Qin (1987)	Dog-bone	70 × 70 × 148/40 × 40 100 × 100 × 210/70 × 70	Unnotched Unnotched	Fixed Fixed	17–34	Ambient
Phillips and Binsheng (1993)	Dog-bone	100 × 150 × 700/100 × 100	Both	Fixed	27–64	Ambient
Rossi et al. (1994)	Cylinder	74 × 100	Unnotched	Fixed	—	Ambient
Mechtcherine et al. (1995)	Dog-bone, prism	$a_1 \times b_1 \times H/60 \times 100$ 60 × 100 × H	Unnotched Notched	Fixed Fixed	43, 53	Ambient
van Vliet and van Mier (1999)	Dog-bone	$a_1/H = 1.5$	Unnotched	Rotating	42	Ambient
Felicetti and Gambarova (1999)	Cylinder	100 × 150	Notched	Fixed	72, 95	105–500 (R)
Felicetti et al. (2000)	Cylinder, dumbbell	64 × H $D_1 \times H/D_2$	Notched Notched	Fixed Rotating	90	20–600 (H, R)
Zheng et al. (2001)	Prism	100 × 100 × 500	Unnotched	Rotating	24–58	Ambient
Kim and Reda Taha (2014)	Cylinder	100 × 200	Unnotched	Fixed	25, 40, 55	Ambient
Lam and Fang (2014)	Dumbbell	80 × 665/60	Unnotched	Rotating	C40, C50, C60	20–800 (H)

Note: Sizes are as follows: dog-bone = $a_1 \times b_1 \times H/a_2 \times b_2$; cylinder = $D \times H$; prism = $a \times b \times H$; and dumbbell = $D_1 \times H/D_2$. Temperature is as follows: ambient = 20°C; R = residual conditions; and H = hot conditions.

Table 2. Summary of the experimental campaign

Specimen ID	UPV test	E_{static} test		Thermal treatment				UCT	UTT
		(ISO 1920-10)	200°C	400°C	600°C	800°C			
C20-1	Y	Y	—	—	—	—	—	Y	—
C20-2	Y	Y	—	—	—	—	—	Y	—
C20-3	Y	Y	—	—	—	—	—	Y	—
C200-1	Y	Y	Y	—	—	—	—	Y	—
C200-2	Y	Y	Y	—	—	—	—	Y	—
C200-3	Y	Y	Y	—	—	—	—	Y	—
C400-1	Y	Y	—	Y	—	—	—	Y	—
C400-2	Y	Y	—	Y	—	—	—	Y	—
C400-3	Y	Y	—	Y	—	—	—	Y	—
C600-1	Y	Y	—	—	Y	—	—	Y	—
C600-2	Y	Y	—	—	Y	—	—	Y	—
C600-3	Y	Y	—	—	Y	—	—	Y	—
C800-1	Y	Y	—	—	—	—	Y	Y ^a	—
C800-2	Y	—	—	—	—	—	Y	Y ^a	—
C800-3	—	—	—	—	—	—	Y ^b	Y ^a	—
C800-4	—	—	—	—	—	—	Y ^b	Y ^a	—
T20-1	—	—	—	—	—	—	—	—	Y
T20-2	—	—	—	—	—	—	—	—	Y
T200-1	—	—	Y	—	—	—	—	—	Y
T200-2	—	—	Y	—	—	—	—	—	Y
T400-1	—	—	—	Y	—	—	—	—	Y
T400-2	—	—	—	Y	—	—	—	—	Y
T600-1	—	—	—	—	—	Y	—	—	Y
T600-2	—	—	—	—	—	Y	—	—	Y

Note: UPV = ultrasonic pulse velocity; E_{static} = static modulus of elasticity; UCT = uniaxial compressive test; and UTT = uniaxial tensile test.

^aOnly peak strength data available.

^bTested in hot conditions.

fracture energy (G_f) in residual conditions. Different temperatures up to 400°C were investigated, showing a changing behavior of G_f with temperature. A decreasing trend was obtained for temperatures below 250°C, while an increasing trend was found from 250°C to 400°C.

The effect of elevated temperatures on specific compressive fracture energy (G_{fc}) was investigated in Felicetti and Gambarova (1998). They reported a decreasing behavior of G_{fc} with temperature. The published data was expressed in terms of dissipated energy per unit of volume. This disagrees with Nakamura and Higai (2001), who performed a series of compressive strength tests at room temperature comparing different H/D ratios. They found that the fracture zone length is almost constant for $H/D > 3$, concluding that the fracture zone is localized over a certain length.

Neuenschwander et al. (2016) performed controlled cyclic compression tests at elevated temperatures (in hot conditions) in order to study the evolution of unloading stiffness with increasing plastic straining. However, results were not obtained for temperatures between 20°C and 500°C, where the decrease in strength and modulus of elasticity is more pronounced. Moreover, experimental damage evolution laws were not found for tensile behavior in the literature. Nechnech et al. (2002) developed an elastoplastic damage model for plain concrete subjected to high temperatures. This model was implemented in the present study using the material parameters obtained from the experiments performed. The predicted damage evolution in tension using the model is compared to the measured values in the “Discussion of Results” section.

Experimental Procedure Description

A total of 20 concrete cylinders were tested in residual conditions after a thermal cycle (in unrestrained conditions) at four different

temperatures (20°C, 200°C, 400°C, and 600°C); a total of 12 standard ($D = 100$ mm, $H = 200$ mm) cylinders were used to test modulus of elasticity and uniaxial compressive strength, while eight cylinders ($D = 100$ mm, $H = 100$ mm) were used for measuring direct uniaxial tensile strength. In addition, four standard ($D = 100$ mm, $H = 200$ mm) cylinders were tested for their uniaxial compressive strength at 800°C. Table 2 presents an overview of the experimental campaign.

Materials

The concrete used has a cylindrical compressive strength (f_c) of 73 MPa, a water-cement ratio (w/c) of 0.42, and a maximum aggregate size (d_{max}) of 16 mm. Table 3 details the concrete mix design. The aggregates (siliceous) are composed of granite, gneiss, sandstone, and siltstone. Polypropylene microfibers were also added into the mix (1 kg/m³). The concrete cylinders were demolded 24 h after casting, cured in water for 28 days, and rested for five to six months at 20°C in a lab environment. The density (ρ) at 28 days was equal to 2,370 kg/m³.

Table 3. Concrete mix design

Material	Content (kg/m ³)
CEM II/B-M 42.5R	223.40
CEM II/A-V 42.5N	193.33
Silica fume	12.89
Water	174.13
Aggregate 8–16	754.95
Aggregate 0–8	1,026.48
Acrylic superplasticizer	3.06
Set-retarding admixture	0.64
Polypropylene fibers	1.00

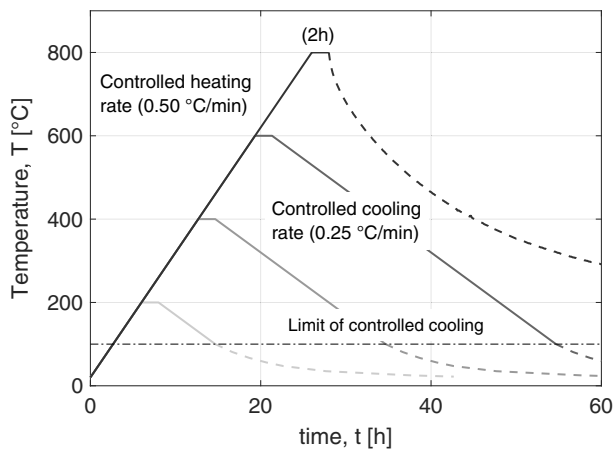


Fig. 1. Temperature cycles at 200°C, 400°C, 600°C, and 800°C.

Heating of Specimens

The concrete cylinders were tested after exposure to four different temperatures: 20°C (room temperature), 200°C, 400°C, and 600°C. Mechanical properties were tested in residual conditions, i.e., with a cooling phase after the heating phase. Specimens were not dried before the thermal treatment. To avoid excessive thermal gradients, the heating and cooling rates were chosen as 0.5 and 0.25°C/min, respectively. Specimens were heated in unrestrained conditions until the maximum temperature was reached, with a stabilization phase of 2 h to ensure a uniform temperature distribution. Afterward, the cooling rate was applied until the specimen reached 100°C, when the furnace was switched off and the specimen naturally cooled in a closed furnace environment (Fig. 1). Other studies by Felicetti and Gambarova (1998), and Colombo et al. (2010) adopted a similar procedure. Specimens for the preliminary tests at 800°C were subjected to the same heating rate. After, they naturally cooled in a closed furnace environment. Spalling was not observed for any specimen during the thermal cycles.

Ultrasonic Pulse Velocity Measurements

Direct ultrasonic pulse velocity (UPV) measurements were taken using an UPV measuring equipment (E49, CONTROLS Group, Liscate, Italy), with two piezoelectric transducers (emitter and receiver) placed on opposite faces of the cylinder, as shown in Fig. 2. Gel was added between the transducer and the concrete face to ensure full acoustic contact. Measurements were taken before and after the thermal cycles for each of the 12 cylinders tested in compression.



Fig. 2. Direct UPV measurements.

The propagation of ultrasonic waves through material is commonly used as a dynamic method to determine the level of internal damage, which can be expressed as Eq. (1) (Lemaitre and Chaboche 1990)

$$D = 1 - \tilde{E}/E \quad (1)$$

where E and \tilde{E} = modulus of elasticity before and after the thermal cycle, respectively. The pulse velocity (v_L) can be expressed as indicated in Eq. (2)

$$v_L^2 = \frac{E}{\rho} \frac{1 - \nu}{(1 + \nu)(1 - 2\nu)} \quad (2)$$

Assuming the isotropic damage hypothesis, constant Poisson's ratio (ν) of 0.2, and neglecting the change in density (ρ), which was found to be less than 10% at 800°C, the level of damage can be then expressed in terms of longitudinal waves velocity as Eq. (3)

$$D = 1 - \tilde{v}_L^2/v_L^2 \quad (3)$$

where v_L and \tilde{v}_L = pulse velocities before and after the thermal cycle, respectively.

Uniaxial Compressive Strength and Modulus of Elasticity Tests

This section describes two different sets of experiments with temperatures up to 600°C and 800°C, respectively. The former involves 12 specimens to test the modulus of elasticity and uniaxial compressive strength. Three nominal identical specimens were tested for each temperature level (20°C, 200°C, 400°C, and 600°C). In the latter, four specimens were used to get a preliminary comparison between the uniaxial compressive strength in hot and residual conditions (Table 2). Specimens were tested using a servohydraulic press (Advantest 9, CONTROLS Group, Liscate, Italy), with a maximum capacity of 3,000 kN. The end-sections of the cylinders were ground to guarantee face parallelism and planarity at the specimen-machine interface.

The static modulus of elasticity of the concrete was evaluated from the displacements measured by means of three linear variable displacement transducers (LVDTs) assembled at 120° astride the central part of the specimen, with a gauge length of 35 mm (Fig. 3). Tests were load controlled, with a loading/unloading rate of 2 kN/s, in accordance with ISO 1920-10 (ISO 2010).

The uniaxial compressive tests were performed under displacement control using the signal of a displacement transducer that could measure the relative displacement between machine platens. The displacement-controlled procedure made it possible to measure the complete stress-strain curves, even in the softening phase. A constant displacement rate of 50 $\mu\text{m/s}$ was used in the elastic region.

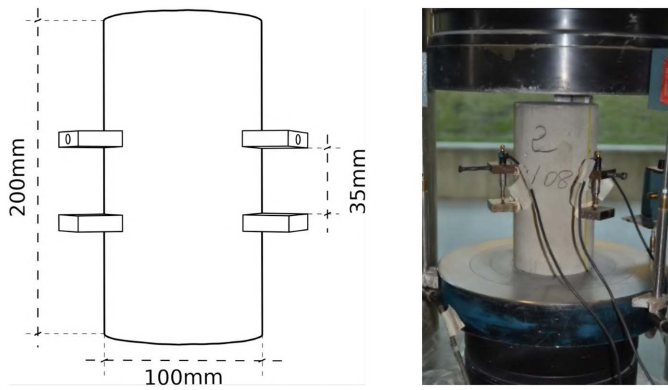


Fig. 3. Instrumentation for modulus of elasticity tests.

A rate of $30 \mu\text{m/s}$ was used during the prepeak and postpeak states, and of $70 \mu\text{m/s}$ during the last part of the softening branch. The relative displacement of the platens, corresponding to the shortening of the specimens, was measured by means of three LVDTs. Unloading-reloading cycles were performed during the tests, measuring the evolution of the stiffness for each temperature. The specific compressive fracture energy was calculated as the area under the stress-strain curve per unit of cross-section area, without the contribution of the elastic unloading part (Felicetti and Gambarova 1999).

Additional uniaxial compression tests were performed at 800°C . Two standard cylinders were tested at high temperature (hot conditions, fast extraction), and two cylinders were tested after cooling (residual conditions). The modulus of elasticity was measured in one of the cylinders in residual conditions.

Uniaxial Tensile Tests

Eight cylinders were tested in uniaxial tension by controlling the crack opening displacement (COD), using an electromechanical press (8562, INSTRON, High Wycombe, UK) with 100 kN capacity. Two nominal identical specimens were tested for each temperature load. The end-sections of the concrete cylinders were ground to guarantee parallelism and planarity in the specimen-machine interaction. A circumferential notch (depth 10.8 mm, width 3.7 mm) was cut in the central part of the specimen after the thermal cycle to guarantee a localized crack. Five LVDTs were mounted at 120° in the central region astride the notch with a gauge length of 40 mm to measure

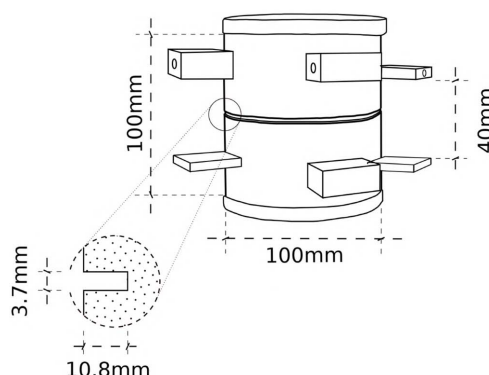


Fig. 4. Instrumentation for uniaxial tensile tests.

the COD. Fig. 4 shows the geometry of the specimen and the instrumentation used during the tests.

Steel plates were attached to the end-sections of the cylinders by means of a thin layer of epoxy glue with a 24-h hardening period and connected with free-rotational heads to the machine. The tests were carried out at a constant COD rate of $0.1 \mu\text{m/s}$ during the loading branch, and $0.2 \mu\text{m/s}$ during the afterpeak softening branch. The displacement rate was progressively increased to 0.5 , 1.0 , and $5.0 \mu\text{m/s}$ during the last part of the softening branch, until complete separation of the specimen into two parts. Control of the COD made it possible to measure the complete stress-crack opening (ω_c) curves. Unloading-reloading cycles were performed during the postpeak part of the tests. The specific tensile fracture energy was calculated as previously described in the section “Uniaxial Compressive Strength and Modulus of Elasticity Tests.”

Evolution of Internal Damage

The unloading-reloading cycles performed during the uniaxial compressive and tensile tests allowed us to study the evolution of unloading stiffness. This material property can be correlated to internal damage using Eq. (1). The evolution of mechanical ($D_{c,i}$) and total ($D_{c,T}$) compressive internal damage is obtained as indicated in Eqs. (4) and (5), respectively

$$D_{c,i} = 1 - K_{c,i,T}^{unl} / K_{c,max,T}^{unl} \quad (4)$$

$$D_{c,T} = 1 - K_{c,i,T}^{unl} / K_{c,max,20}^{unl} \quad (5)$$

where $K_{c,i,T}^{unl}$ = compressive unloading stiffness for an exposure temperature (T) for each unloading-reloading cycle (i); $K_{c,max,T}^{unl}$ = maximum compressive unloading stiffness for the temperature (T); and $K_{c,max,20}^{unl}$ = maximum compressive unloading stiffness of the reference case (20°C). The evolution of mechanical ($D_{ct,i}$) and total ($D_{ct,T}$) tensile internal damage is obtained as indicated in Eqs. (6) and (7), respectively

$$D_{ct,i} = 1 - K_{ct,i,T}^{unl} / K_{ct,o,T}^{unl} \quad (6)$$

$$D_{ct,T} = 1 - K_{ct,i,T}^{unl} / K_{ct,o,20}^{unl} \quad (7)$$

where $K_{ct,i,T}^{unl}$ = tensile unloading stiffness for an exposure temperature (T) for each unloading-reloading cycle (i); $K_{ct,o,T}^{unl}$ = initial tensile unloading stiffness for the temperature (T); and $K_{ct,o,20}^{unl}$ = initial tensile unloading stiffness of the reference case (20°C).



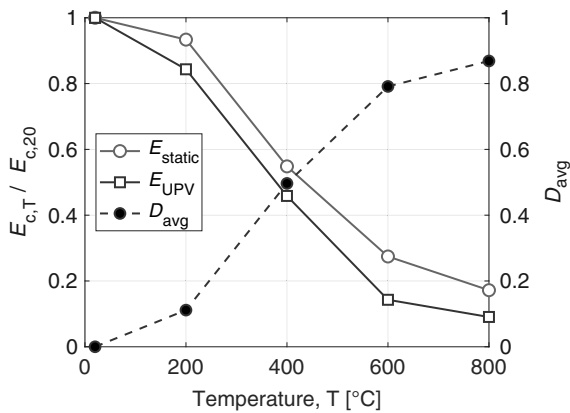


Fig. 5. Relative modulus of elasticity and damage for different temperatures after cooling.

Results

Modulus of Elasticity of Concrete

Fig. 5 compares the evolution of the static and the dynamic (UPV) modulus of elasticity. The dashed line denotes the evolution of internal damage caused by the thermal treatment. As shown, both methods confirm the significant decrease in the modulus of elasticity in concrete subjected to high temperature. On average, from

20°C to 200°C, the modulus is slightly reduced until $0.90E_{c,20}$. Between 200°C–400°C and 400°C–600°C, the material suffers a faster reduction, reaching $0.50E_{c,20}$ and $0.20E_{c,20}$, respectively. Above 600°C, the reduction of the modulus is less pronounced, reaching $0.15E_{c,20}$ at 800°C. Comparing the two methods, the modulus of elasticity obtained using the dynamic method is higher at 20°C and 200°C than the static method. Nevertheless, Fig. 5 reveals how the dynamic method has a more pronounced decrease.

Compressive Behavior of Concrete

Fig. 6 shows the complete nominal stress-strain curves obtained during the compressive strength tests carried out after cooling. Each plot shows three different curves, corresponding to the three nominally identical tests, and an additional average curve. The slope of stress-strain curve decreases with increasing temperature because of a decrease in the maximum nominal stress and an increase of the strain at peak stress (ϵ_{c1}). This effect is linked to the reduction of stiffness observed in Fig. 5.

As seen in Fig. 6, only a few points of the afterpeak part of the curve were recorded for the temperatures of 20°C and 200°C. The stress-strain curves for those temperatures were therefore extended using the CEB-FIP predicting model [fib 1 (fib 1990)], which is a modified form of the model proposed by Sargin and Handa (1969). The extensions are shown as dashed lines in Fig. 6. Furthermore, measurements from the relative displacement of the platens include undesired additional stresses due to the end-effects,

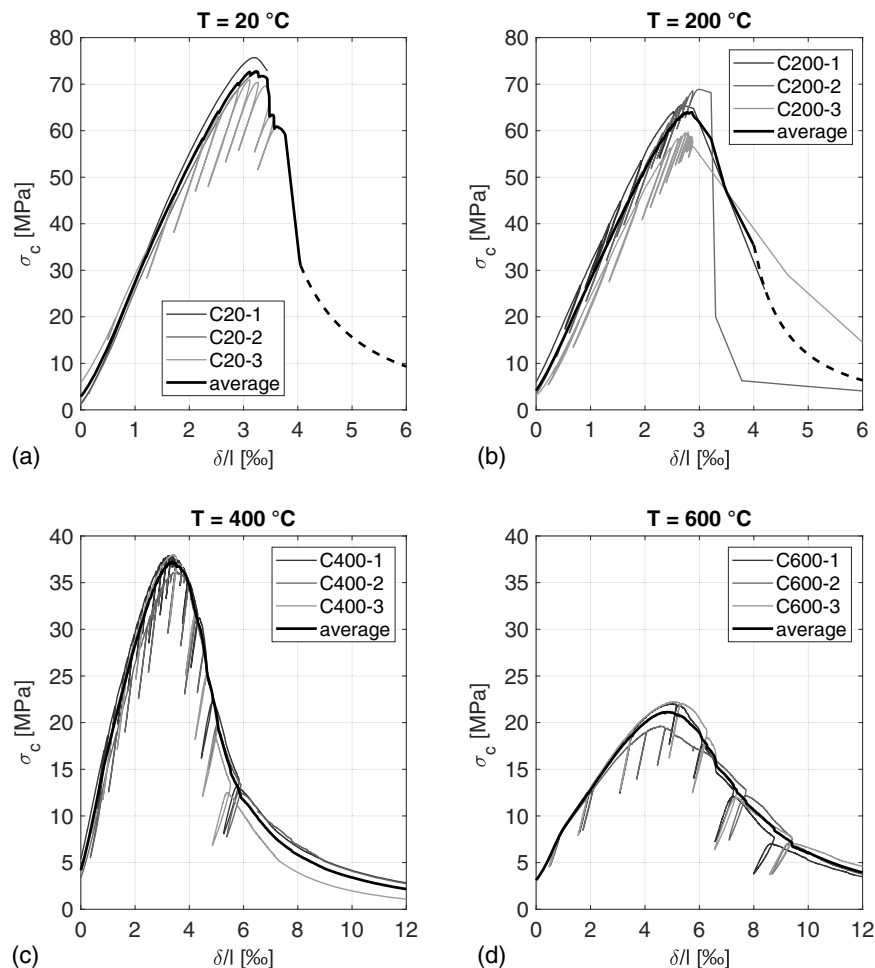


Fig. 6. Compressive nominal stress-strain curves for different temperatures after cooling.

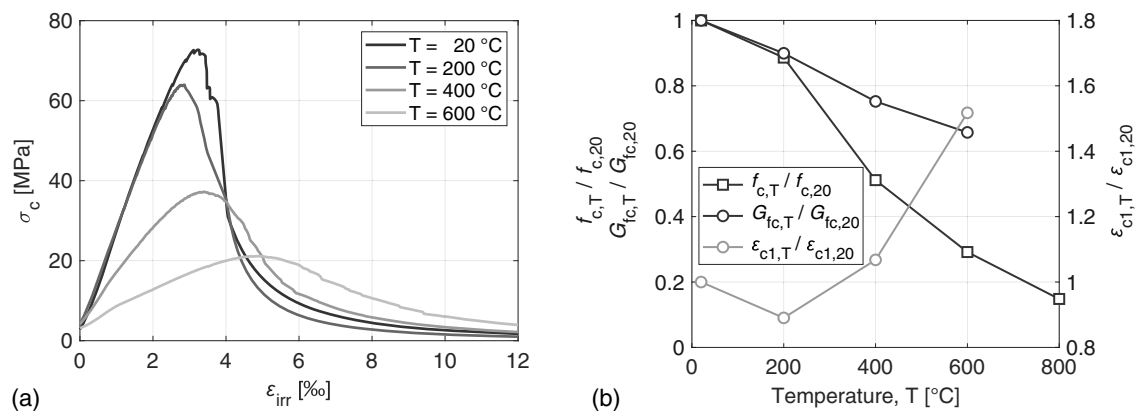


Fig. 7. (a) Average compressive stress-strain curves; and (b) evolution of nominal compressive peak strength, specific compressive fracture energy, and strain at peak stress, after cooling.

and eccentricity. To compensate for this effect, the stress-strain curves were shifted by using the first unloading cycle performed. Note that these results cannot directly be compared to the material model proposed in the new version of the Eurocode 2 Part 1–2 (CEN 2019). The reason is that the model, unlike the shown experimental curves, incorporates the effects of transient creep occurring during heating of a structure under a certain load.

Fig. 7(a) compares the average nominal stress-strain curve from all four temperatures after cooling. Fig. 7(b) shows the evolution of the nominal compressive strength, specific compressive fracture energy, and strains at peak stress for the different temperatures. In Figs. 7(a and b), the values are normalized with the corresponding values evaluated in room-temperature conditions. Fig. 7(b) also includes the result of compressive strength for the specimens heated to 800°C. Fig. 7(b) shows that exposure to elevated temperatures significantly reduces the compressive strength of concrete, with a trend similar to that observed for the modulus of elasticity (Fig. 5). The average compressive peak strength from the three tests at 20°C is 73.0 MPa. After exposure to elevated temperatures, the residual peak strength decreases to approximately $0.90f_{c,20}$ after 200°C, $0.50f_{c,20}$ after 400°C, and $0.30f_{c,20}$ after 600°C. The residual compressive peak strength after 800°C decreases to $0.15f_{c,20}$.

As shown in Fig. 7(b), G_{fc} after 200°C is $0.90G_{fc,20}$. The reduction after higher temperatures reaches $0.75G_{fc,20}$ and $0.65G_{fc,20}$ at 400°C and 600°C, respectively. However, ϵ_{c1} shows a significant increase with temperature. While the strain after 200°C is 10% less than at 20°C, it increases by approximately 7% and 50% at 400°C and 600°C, respectively. This effect is related to the reduction in stiffness, as previously mentioned. The average compressive strength obtained for exposure to 800°C was 13.0 MPa in hot conditions and 10.8 MPa in residual conditions. This represents a decrease of approximately 20% during the cooling phase.

Tensile Behavior of Concrete

Fig. 8 shows the nominal stress-crack opening curves for the tensile tests at different temperatures after cooling. Results of the two nominally identical tests are shown for each case, together with the average curve. As seen, the stress-crack opening curve becomes flatter when increasing in temperature. Microcracking in the specimen due to the thermal treatment causes a reduction of the initial stiffness. This effect is well illustrated in Fig. 9(a), especially for temperatures of 400°C and 600°C, where the average curve for all four different temperatures are compared. Moreover, cycles of

unloading-reloading in the softening part show a stiffness reduction as ω_c increases.

Fig. 9(b) shows the evolution of the normalized tensile strength, the specific tensile fracture energy, and the crack opening at peak stress after cooling from the different temperature levels. The maximum stress reached at 200°C is about 20% higher than the maximum stress at 20°C. This phenomenon is studied in the “Discussion of Results” section, which compares these results with those of other research studies. Above 200°C, the residual peak tensile strength significantly decreases to approximately $0.70f_{ct,20}$ for 400°C and $0.30f_{ct,20}$ for 600°C.

Fig. 9(a) shows how the peak stress tends to decrease with higher temperatures, while the curve becomes flatter, therefore reaching higher ω_c during the postpeak part. In contrast, the complete split of the specimen occurs at a lower ω_c at room temperature. This effect is reflected in Fig. 9(b), which shows how the specific fracture energy increases with temperature and reaches approximately $1.40G_{f,20}$ at 600°C. As shown, ω_{c1} significantly increases with temperature, reaching $2.25\omega_{c1,20}$ at 600°C.

Damage Evolution

Figs. 10(a and b) show the evolution of mechanical ($K_{c,i,T}^{unl}/K_{c,max,T}^{unl}$) and total ($K_{c,i,T}^{unl}/K_{c,max,20}^{unl}$) unloading stiffness in compression for each exposure temperature, with the irreversible strain (ϵ_{irr}). Note that only a few unloading cycles were performed for 20°C and 200°C (Fig. 6) because the afterpeak behavior could not be recorded. The experimental results are shown as markers, while continuous lines represent the fitting curves. Dashed lines highlight the maximum value for each fitting curve.

Fig. 10(b) presents the combined effect of thermal and mechanical loading on the evolution of unloading stiffness, by comparing it to the maximum unloading stiffness at 20°C ($K_{c,max,20}^{unl}$). The thermal loading results in a reduction of unloading stiffness equal to 59% of the maximum stiffness for the specimen at 600°C. Both thermal and mechanical loading have a significant influence at 400°C, where the maximum stiffness reduction represents 28% of the total reduction. Less significant maximum stiffness reduction is observed at 200°C, just 9% of the total reduction.

Figs. 11(a and b) show the evolution of mechanical ($D_{ct,i}$) and total ($D_{ct,T}$) internal damage in tension for each exposure temperature, together with $\omega_{c,irr}$. The obtained results are shown as markers, while continuous lines represent the fitting curves.

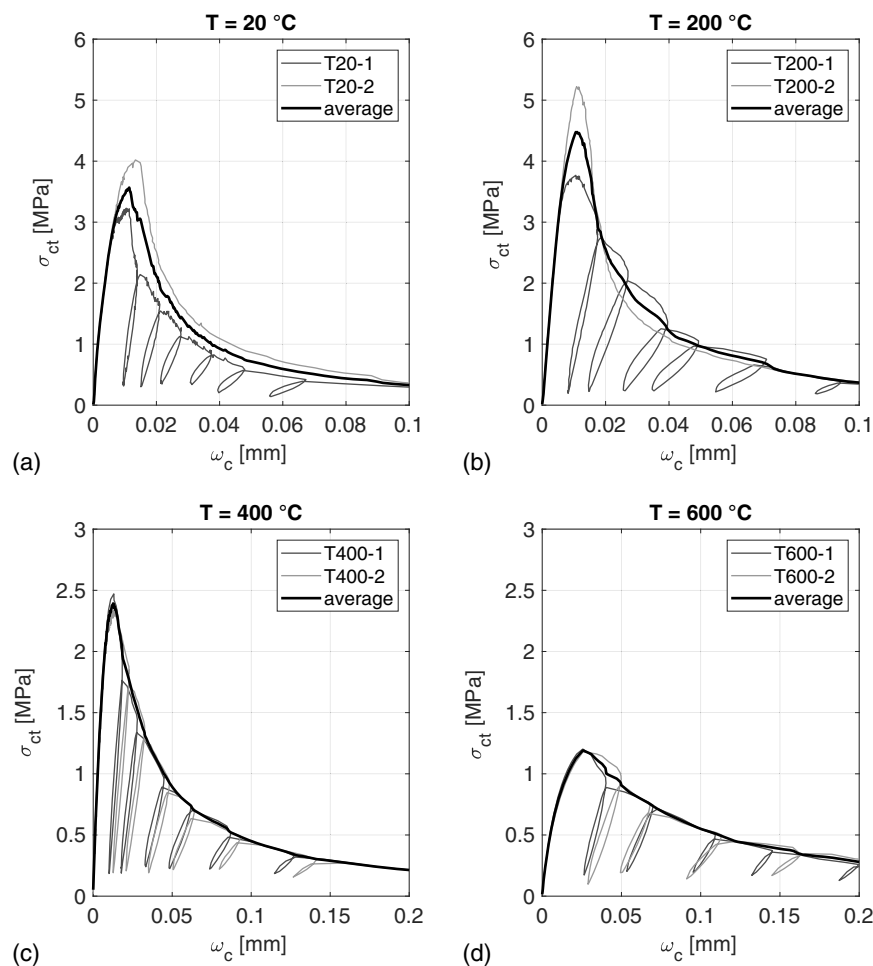


Fig. 8. Tensile nominal stress-crack opening curves for different temperatures after cooling.

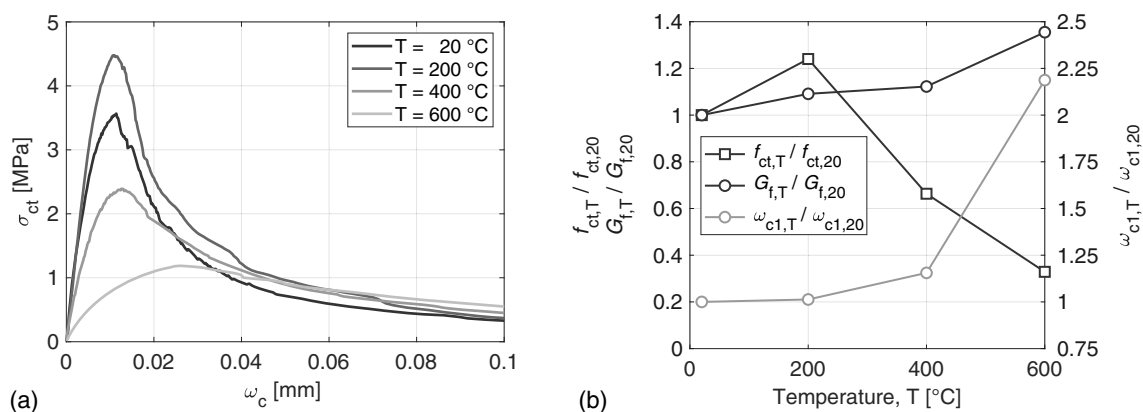


Fig. 9. (a) Average tensile stress-crack opening curves; and (b) evolution of tensile nominal peak strength, specific tensile fracture energy, and crack opening at peak stress after cooling.

As seen in Fig. 11(a), the mechanical damage significantly increases up to $\omega_{c,irr} = 0.020$ mm, reaching 80%, 86%, 74%, and 70% at 20°C, 200°C, 400°C, and 600°C, respectively. As with the evolution of mechanical damage in compression, the degree of damage for a given $\omega_{c,irr}$ decreases as the maximum exposure temperature increases. However, the opposite effect is observed between exposure temperatures of 20°C and 200°C, up to $\omega_{c,irr} = 0.035$ mm.

Fig. 11(b) presents the combined effect of thermal and mechanical loading on the evolution of damage. The irreversible thermal loading has a greater effect in tension than in compression for temperatures of 400°C and 600°C, while it is similar at 200°C. The initial thermal damage represents 76% of the total damage at 600°C, which clearly shows the small contribution of mechanical loading during the test. At 400°C, the thermal loading has a

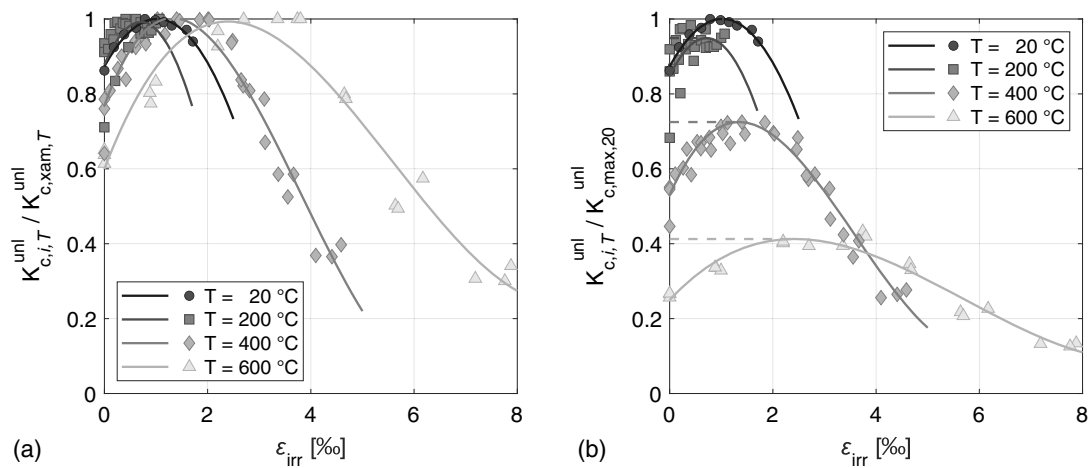


Fig. 10. Evolution of (a) mechanical; and (b) total unloading stiffness in compression.

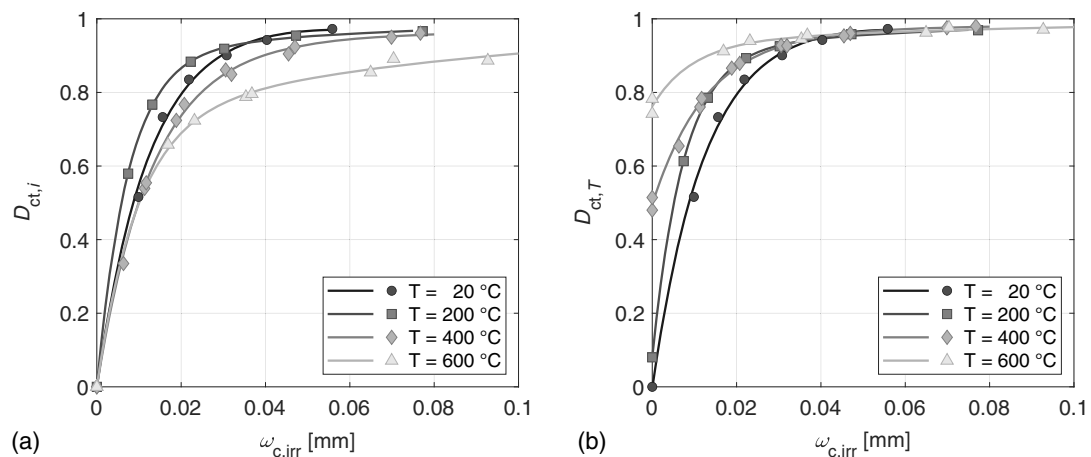


Fig. 11. Evolution of (a) mechanical ($D_{ct,i}$); and (b) total ($D_{ct,T}$) internal damage in tension.

significant effect on the initial thermal damage, equal to 50% of the total damage. A relatively low initial thermal damage of 9% was induced by a thermal loading of 200°C.

Discussion of Results

This section discusses the results we obtained for the influence of temperature on the residual compressive and tensile strengths, modulus of elasticity, and specific compressive and tensile fracture energies of concrete, comparing them with previous research. Concrete strengths from studies compared in this section are for cylindrical specimens. Where compressive strength was not given, the class of concrete is shown. In the following subsections, relative quantities report the ratio between the value at a certain temperature and the value at room temperature.

In recent years, RILEM has released standard procedures on how to determine properly the influence of high temperature on mechanical properties of concrete such as modulus of elasticity (Schneider et al. 2004), tensile strength (Schneider et al. 2000), and stress-strain curves (Schneider et al. 2007). These procedures mention the case of accident conditions, which normally involve temperatures between 20°C and 750°C, without specifying which temperatures should be used. Testing at elevated temperatures

requires special equipment and the number of samples is normally limited. Such research is therefore commonly narrowed to three or four temperature cases. Studies in the literature use different temperature values and numbers of thermal cycles, which complicates the comparison of results.

Modulus of Elasticity

Fig. 5 displays the relative modulus of elasticity and damage for the different temperatures after cooling. As shown, internal damage increases with temperature, reaching a value close to 0.90 at 800°C. Because of the heterogeneity of concrete, different components experience different thermal strains, which leads to internal thermal stresses causing microcracking that can be considered as a material damage on the scale of the volume of material investigated.

Figs. 12(a and b) show the obtained results for the total and the relative modulus of elasticity, respectively, together with some of the experimental results found in the literature (Felicetti and Gambarova 1998; Khoury et al. 1999; Phan and Carino 2001). A dashed line denotes the results obtained using the dynamic (UPV) method, while the other lines represent results obtained with the static method.

Model Code 2010 (fib 2013) presents a relationship to calculate the modulus of elasticity at room temperature, based on the compressive strength of concrete, $E_{cm} = 21.5(f_{cm}/10)^{1/3}$, which is

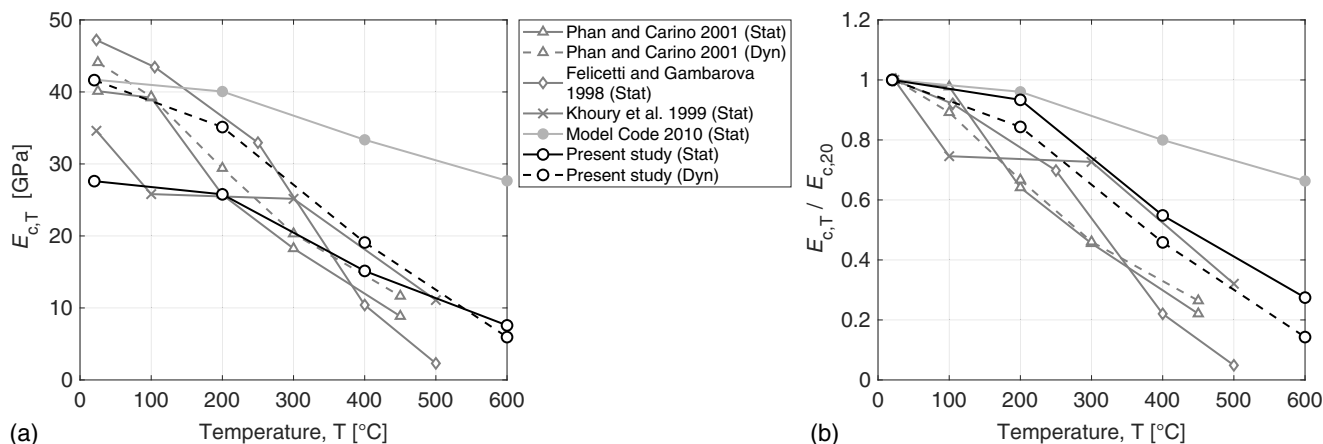


Fig. 12. Experimental results of (a) total; and (b) relative modulus of elasticity after cooling.

very similar to the one proposed in the Eurocode 2 Part 1–1 (CEN 2004a). Because the code does not provide any additional relationship for high temperatures (up to 600°C), this equation was used to calculate the modulus at different elevated temperatures, taking the corresponding reduced strength obtained experimentally. The calculated values are also illustrated in Fig. 12.

The obtained decrease of the modulus confirms the results from other studies. This behavior is mainly related to thermal stresses and physical and chemical changes in the material. The loss of moisture due to heating and the degradation of microstructure and chemical bonds results in the development of microcracks, which causes this pronounced decrease (Khaliq and Kodur 2012). As observed, the values obtained with the relationship from the Model Code 2010 (fib 2013) underestimate the damage on the modulus caused by high temperatures.

The static and dynamic methods present very different procedures. The static calculation of the modulus is based on the increment of the strain within the elastic regime of the stress-strain curve; therefore, it requires the use of a very accurate transducer to achieve representative results. Conversely, the dynamic method is a relatively simple procedure with UPV measurements. The obtained results with the latter are in agreement with Phan and Carino (2001), and Felicetti and Gambarova (1998), who also reported a significant reduction between 200°C and 400°C. Moreover, the results obtained at 300°C and 500°C agree with the findings reported by Khoury et al. (1999).

The load applied using the static method induces immediate creep in the specimen. Therefore, a higher displacement is measured, resulting in a lower modulus of elasticity. This effect is well illustrated in Fig. 12(a) comparing the results from the two methods reported by Phan and Carino (2001). For this reason, the dynamic method sometimes gives a more meaningful measure of the temperature effect on the elastic response of concrete (Bazant 1976). However, Phan and Carino (2001) reported a decrease in stiffness at 100°C, which is higher using the dynamic method compared with the static method [Fig. 12(b)]. It was shown that voids formed by the loss of absorbed, capillary, and interlayer water can cause a higher decrease of UPV measurements, which was not obtained using static tests (Ghandehari et al. 2010). Therefore, in the present study an additional cylinder was heated to 110°C, taking UPV measurements before and after the thermal treatment. The contribution of the water, quantified as 7.2% of the total, was then subtracted from all the UPV measurements on nonheated specimens, in order to have a more realistic comparison between the two methods.

Based on the compared results, we conclude that the dynamic method with UPV readings is a better way to measure the modulus of elasticity, being a noninvasive simple procedure and providing values more similar to other studies. However, measurements at lower temperatures may give an overestimation of the modulus due to the contribution of water. Stress analysis in numerical simulations could be influenced by the modulus used. Therefore, it is best to input the entire stress-strain curve, in both compression and tension for the whole temperature range, as provided in this study. Furthermore, the relationship proposed by the Model Code 2010 (fib 2013) at room temperature should not be used to predict the modulus of elasticity at high temperatures, because it is shown to underestimate the damage on the stiffness, contrary to the significant decreasing tendency found in the present study and previously reported in the literature.

Compressive Behavior

Fig. 13 displays our results for the relative compressive strength with the experimental results for residual conditions found in the literature. The measured values show a similar trend as those from the literature, confirming the significant decrease in the residual peak compressive strength of concrete at elevated temperatures. This decrease is less pronounced than for the modulus of elasticity. As shown, the range between 200°C and 400°C is the interval where the reduction is most pronounced, which is mainly linked to the increased porosity and microcracking in the material (Khoury 1992).

Fig. 13 shows that the results obtained in the present work for temperatures up to 200°C are similar to those shown in the new draft of Eurocode 2 Part 1–2 (CEN 2019). Nevertheless, the code tends to overestimate the residual peak compressive strength for the temperatures up to 800°C. The review presented in Shah et al. (2019) remarked that most studies report unsatisfactory agreement between their test results and the standards. There is a need to quantify the applicability of the Eurocode recommendations for HSC exposed to fire, which should consider the influence of the parameters reported by RILEM (Pimienta et al. 2019), such as the initial compressive strength, the concrete mixture, or the content of PP microfibers.

Tensile Behavior

Tests on nonheated specimens presented in the “Results” section, resulted in a lower tensile strength than specimens that had been

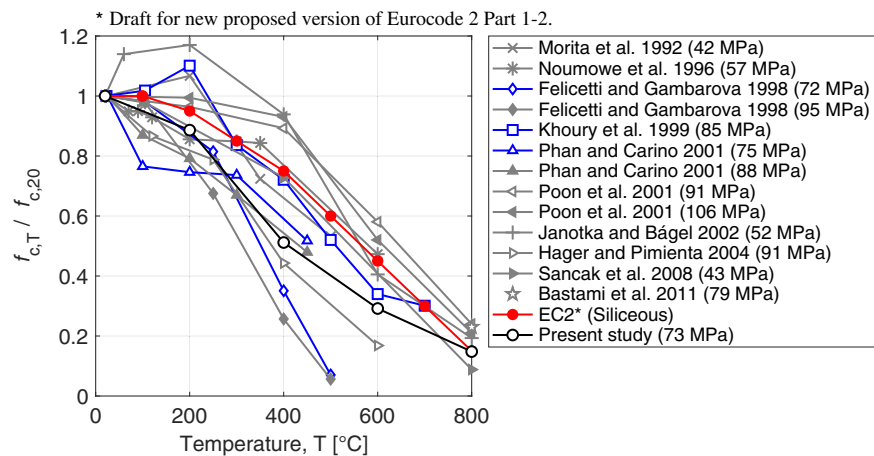


Fig. 13. Experimental results of relative compressive strength at different temperatures after cooling.

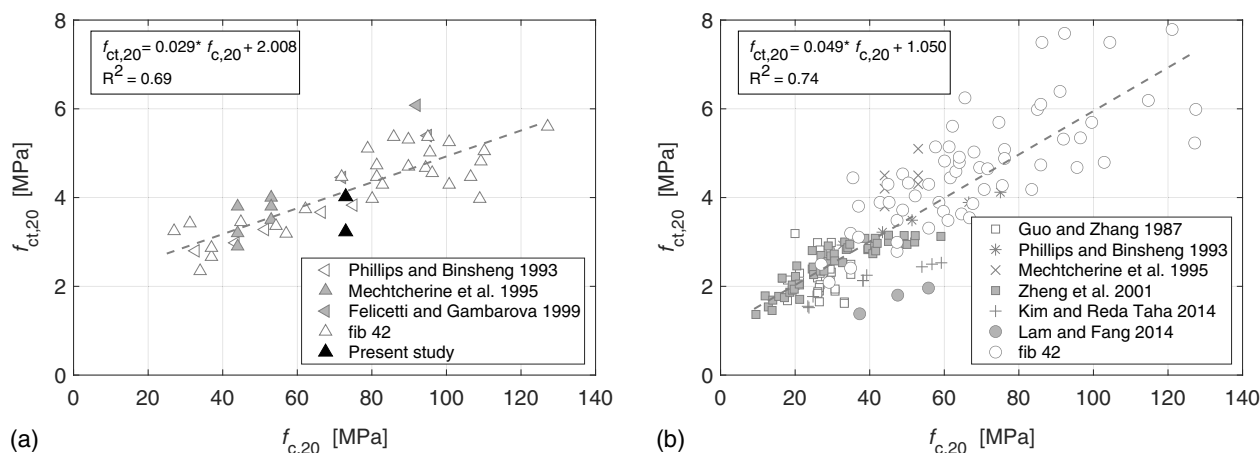


Fig. 14. Scatter of uniaxial tensile tests at 20°C on (a) notched; and (b) unnotched specimens characterized by different concrete strength.

heated to 200°C. A possible explanation for this is the considerable scatter in the uniaxial tensile test results. For this reason, the results from the tests performed at room temperature are first discussed. Fig. 14 shows tensile strength test results at 20°C for specimens differing in compressive strength, corresponding to the various experimental results from the literature. The results are shown separately depending whether the test was performed on notched or unnotched specimens [Figs. 14(a and b), respectively].

There is considerable scatter in the results for both types of specimen, but with a common trend. The scatter may be due to different boundary conditions, i.e., the attachment between steel plates and specimen, and different specimen shapes. Note that notched specimens generally display less strength than unnotched specimens. Fig. 14(a) shows that the results we obtained, though in line with the overall results, are statistically lower than those from other studies.

Figs. 15(a and b) show our results for the total and the relative uniaxial tensile strength, respectively, together with those from other studies in the literature. As seen, the results found in the present work partially agree with the study performed by Felicetti and Gambarova (1999). Our result for tensile strength at room temperature differs from their results. Note that the tests were not performed in the same way. Felicetti and Gambarova (1999) used 100 × 300 mm notched specimens with fixed ends, while our tests

were on 100 × 100 mm specimens with free-rotational ends. The difference in the values obtained may be due to the different end restraints of specimens, and the scatter previously shown in Fig. 14(a). Moreover, the residual peak strengths obtained at high temperatures are significantly higher (30%–40%), than those reported by Felicetti and Gambarova. This may be due to the different specimen's aspect ratio, equal to 1:1 in our study and 1:3 in Felicetti and Gambarova (1999).

Based on the comparison of results, we conclude that the new draft of Eurocode 2 Part 1–2 is in accordance with the behavior of this type of HSC in tension at high temperatures, after cooling. The results confirmed the significant decrease in uniaxial tensile strength of specimens subjected to high temperatures, nearing $0.30f_{ct,20}$ after exposure to 600°C. Moreover, uniaxial tensile tests lead to greater scatter in results compared to other tensile strength tests, mainly due to the boundary conditions and the interaction between the steel and the specimen, which can induce secondary stresses.

Fracture Energy

Evolution of Specific Tensile Fracture Energy

Figs. 16(a and b) compare the evolution of the specific tensile fracture energy with temperature as found in the present work with that

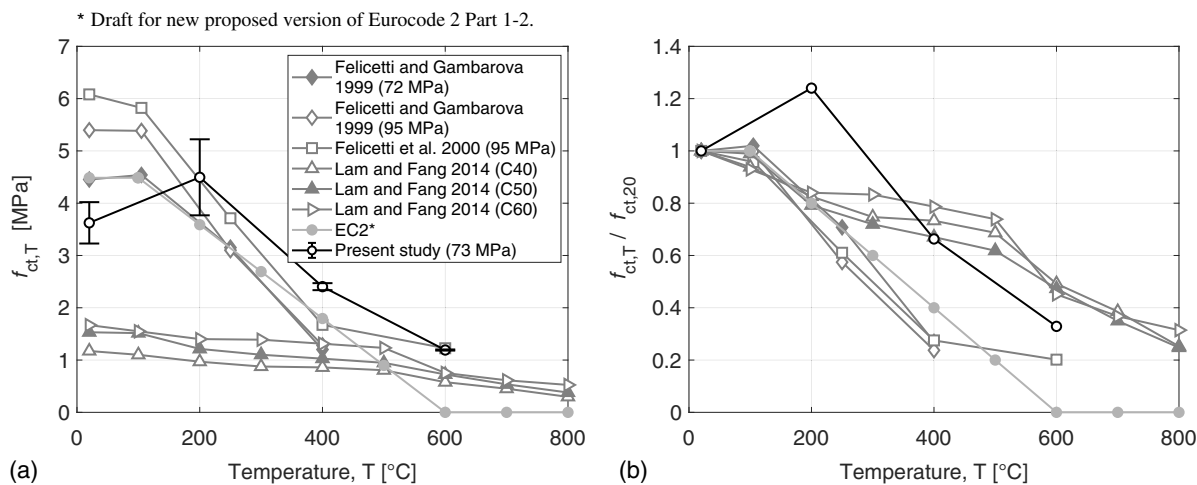


Fig. 15. Experimental results of (a) total; and (b) relative tensile strength after cooling.

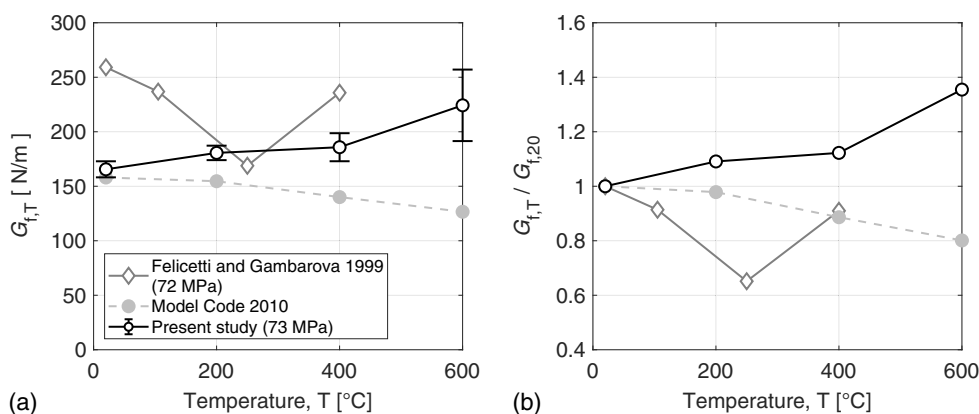


Fig. 16. Evolution of (a) total; and (b) relative specific tensile fracture energy after cooling.

reported by Felicetti and Gambarova (1999). Fig. 16(a) shows that the results obtained in the present study are generally lower than the results presented by Felicetti and Gambarova. The most obvious reason for this is the different boundary conditions used during the tests, which were fixed ends for Felicetti and Gambarova and rotating ends in the present study. A fixed end tensile test results in higher specific fracture energy because the supports absorb some of this energy to compensate the moment caused by any eccentricity. This was previously observed in van Vliet and van Mier (1999), who remarked that when the specimen ends can rotate freely, the boundary influences are minimized, yielding a lower bound for the fracture energy.

Model Code 2010 (fib 2013) proposes a relationship to calculate the specific fracture energy in tension at room temperature, based on the compressive strength of concrete ($G_f = 73f_{cm}^{0.18}$). If this expression is used and $f_{cm} = 73$ MPa, a value of $G_f = 158$ N/m is obtained. This is in line with the averaged results obtained in the present work ($G_f = 166$ N/m). Nevertheless, this relationship should not be used to calculate the specific tensile fracture energy at elevated temperatures, as it leads to inaccurate results (see Fig. 16).

For higher temperatures, the results we obtained partially agree with those presented by Felicetti and Gambarova (1999). Both curves show a similar value for 200°C, and afterward tend to increase for 400°C and 600°C. Fig. 16(a) shows how the difference between each pair of identical tests increases with temperature.

Evolution of Specific Compressive Fracture Energy

Figs. 17(a and b) compare the evolution of specific compressive fracture energy with temperature obtained with the work done by Felicetti and Gambarova (1998). The obtained results agree well with those presented by Felicetti and Gambarova (1998), with similar values for G_{fc} and the similar decreasing tendency for temperatures of 20°C, 200°C, and 400°C. However, the result we obtained for 600°C is higher than the result presented by Felicetti and Gambarova for 500°C. Fig. 17(a) shows how the scatter of the obtained results decreases from 200°C to 600°C, unlike the observations for the G_f [Fig. 16(a)].

Nakamura and Higai (2001) proposed a relationship to calculate the specific compressive fracture energy at room temperature based on the specific tensile fracture energy ($G_{fc} = 250 G_f$). Using the obtained G_f (166 N/m), the G_{fc} is calculated as 41,400 N/m. This value agrees well with the results obtained in the present study ($G_{fc} = 42,215$ N/m) and those of Felicetti and Gambarova ($G_{fc} = 42,000$ N/m). Nevertheless, the presented relationship should not be used to calculate the specific compressive fracture energy at elevated temperatures (see Fig. 17).

Based on the compared results, we conclude that elevated temperatures significantly affect the specific fracture energy. In tension, specific fracture energy increases by up to 35% for 600°C, with additional increase of the scatter of the results. In compression, the behavior is the opposite, where the specific fracture energy

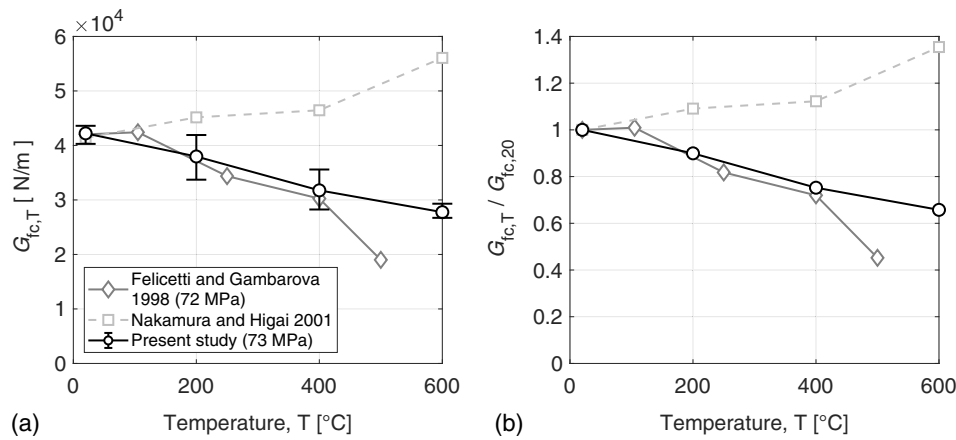


Fig. 17. Evolution of (a) total; and (b) relative specific compressive fracture energy after cooling.

decreases by up to 34% for 600°C, with decreasing scatter. Furthermore, the relationships presented by Model Code 2010 (*fib* 2013) and Nakamura and Higai (2001) provide accurate values of G_f and G_{fc} at room temperature, respectively. However, these relationships are not meant for higher temperatures. Therefore, additional relations should be proposed.

Damage Evolution

Evolution of Internal Damage in Tension

Figs. 18(a and b) compare the evolution of internal damage between the values obtained in the present study (continuous line) with the values obtained using the model proposed by Nechnech et al. (2002) (dashed line). As shown in Fig. 18(a), the predicted values of mechanical damage tend to be higher than the measured values after $\omega_{c,irr}$ of 0.025 mm. This is clearly visible for the case at 600°C, which yields the most disagreement between the model and the experiments. Nevertheless, the influence of the mechanical part into the total damage is less relevant as the temperature increases. Therefore, the evolution of the total (thermomechanical) damage is well predicted by using this analytical model [see Fig. 18(b)].

Based on this comparison, we conclude that the model proposed by Nechnech et al. (2002) could be used to predict the damage evolution in tension. However, certain parameters need to be known, such as tensile strength, specific fracture energy, the initial slope in

softening, and the specific tensile damage variable. These parameters are derived from the stress-COD curves after uniaxial tensile tests with unloading-reloading cycles.

Evolution of Internal Damage in Compression

Fig. 10(a) presents the evolution of the mechanical unloading stiffness during the compressive test, without considering the initial damage produced by the thermal treatment. A similar behavior of stiffness increase is visible at the beginning of all temperature curves, followed by a stiffness reduction. This stiffness increase may be due to the lack of friction reduction lubricant in the compressive strength test, which causes a nonlinear stress state throughout the specimen, due to a frictional constraint at the interface between the material and the loading system. In slender specimens (e.g., $H/D = 2$) failure occurs in the central unconfined regions without significantly affecting the compressive strength value (van Vliet and van Mier 1996). The confinement effect in the end regions of the specimen, which becomes greater as the compression force increases, causes a reduction of plate-to-plate deformation. The action of the confinement is lost when dilatancy becomes dominant. This causes a decrease in the unloading stiffness [see Fig. 10(a)]. As seen, this effect is more efficient when the material is more thermally damaged.

An additional compressive strength test was performed to corroborate this effect, in which friction reduction lubricant was applied. The results confirmed the presence of the confinement

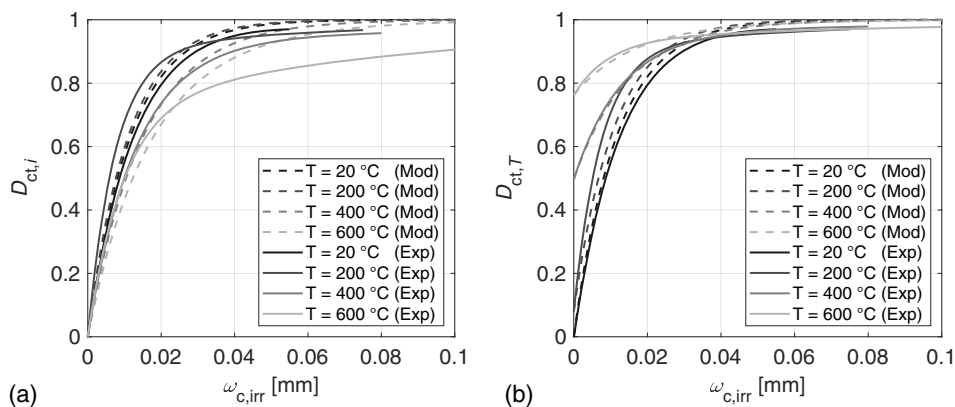


Fig. 18. Comparison of (a) mechanical; and (b) total damage evolution between Nechnech et al. (2002) model (Mod) and the obtained experimental results (Exp).

effect, which alters the unloading stiffness measurements. Therefore, the evolution of internal damage on compressive behavior is presented in terms of stiffness instead of a strictly material property as damage. Moreover, Fig. 10(a) shows that the ratio of unloading stiffness for a given irreversible strain becomes higher as the maximum exposure temperature increases. This is particularly evident when the 400°C and 600°C curves are compared. This effect is due to the reduction in maximum stiffness of the material when subjected to high temperatures.

Conclusions

This study presents a comprehensive approach for the material characterization of a specific type of HSC ($f_c = 73$ MPa) exposed to high temperatures. The effect of elevated temperature on less investigated properties such as the uniaxial tensile strength and the specific compressive and tensile fracture energy was studied. Tests on basic properties such as the modulus of elasticity and the compressive strength were also performed. The measuring of the complete constitutive behavior enabled the investigation of the specific compression and tension fracture energy at elevated temperatures, and the evolution of internal damage. These properties were investigated at 20°C, 200°C, 400°C, and 600°C in residual conditions, with some preliminary results at 800°C. The obtained results were compared with previous research studies and the design codes. Based on this research, the following conclusions can be drawn:

- High temperatures have a significant effect on the combined thermal and mechanical internal damage, for both compression and tensile behavior. In compression, thermal exposure induces an initial irreversible damage equal to 9%, 28%, and 59% of the total unloading stiffness reduction at 200°C, 400°C, and 600°C, respectively. In tension, the initial irreversible damage is equal to 8%, 50%, and 76% of the total damage.
- The model presented by Nechnech et al. (2002) can be used for predicting the evolution of damage of concrete in tension at elevated temperatures, as it yields similar findings compared to results obtained in the present study. Nevertheless, accurate material parameters should be known, being derived from the complete stress-strain curves with unloading cycles.
- The exposure at high temperatures differently affects the tensile and compressive behavior of the specific fracture energy. In tension, it increases up to 35% at 600°C, with additional increase of the scatter of the results. In compression, it decreases to 34% at 600°C, with decreasing scatter.
- Relationships presented by Model Code 2010 (fib 2013) and Nakamura and Higai (2001) provide accurate values of specific tensile and compressive fracture energy respectively, at room temperature. However, these relationships are not meant for higher temperatures, and thus additional relations should be proposed.
- Compared to the static modulus of elasticity, the values of dynamic modulus were more similar to those reported in the literature. The absence of creep and the simple nondestructive procedure make the UPV a more reliable technique to quantify the degradation of the material, after exposure at elevated temperatures. The relationship for the modulus of elasticity at room temperature proposed by the Model Code (fib 2013) should not be used to calculate the stiffness after exposure on this type of HSC, because it is shown to underestimate the damage caused by the elevated temperatures.
- The present study confirmed the significant decrease in compressive strength at high temperatures, where the most pronounced

decrease occurs between 200°C and 400°C. The obtained results of compressive strength are in accordance with the new proposed version of Eurocode 2 Part 1–2 for temperatures up to 300°C. Nevertheless, the results for this type of HSC differ from the code for higher temperatures. Large differences between the published studies and the code remark the need to provide additional information in the recommendations for HSC exposed to fire.

- The results confirmed the significant decrease in uniaxial tensile strength of specimens subjected to high temperatures. This behavior is well described in the new proposed version of Eurocode 2 Part 1–2.

Data Availability Statement

All data, models, and code generated or used during the study appear in the published article.

Acknowledgments

The authors wish to thank Professor Roberto Felicetti for his support during the uniaxial tensile tests. The work presented in this paper is part of an ongoing Ph.D. study funded by the Norwegian Public Roads Administration as part of the Coastal Highway Route E39 project.

References

- Abrams, M. S. 1971. *Compressive strength of concrete at temperatures to 1600 F*. Temperature and Concrete. ACI SP 25-2, 33–58. Detroit: American Concrete Institute.
- Anderberg, Y., and S. Thelandersson. 1976. *Stress and deformation characteristics of concrete: Experimental investigation and material behaviour model*, 86. Lund, Sweden: Univ. of Lund.
- Bastami, M., A. Chaboki-Khiabani, M. Baghadrani, and M. Kordi. 2011. “Performance of high strength concretes at elevated temperatures.” *Sci. Iranica* 18 (5): 1028–1036. <https://doi.org/10.1016/j.scient.2011.09.001>.
- Bazant, Z. 1976. *Review of literature on high temperature behavior of concrete*. Rep. No. ORNL-TM-514s. Oak Ridge, TN: Oak Ridge National Laboratory.
- Bingöl, A. F., A. Tortum, and R. Gül. 2013. “Neural networks analysis of compressive strength of lightweight concrete after high temperatures.” *Mater. Des.* 52 (Dec): 258–264. <https://doi.org/10.1016/j.matdes.2013.05.022>.
- Campbell-Allen, D., and P. M. Desai. 1967. “The influence of aggregate on the behaviour of concrete at elevated temperatures.” *Nucl. Eng. Des.* 6 (1): 65–77. [https://doi.org/10.1016/0029-5493\(67\)90047-7](https://doi.org/10.1016/0029-5493(67)90047-7).
- CEN (European Committee for Standardization). 2004a. *Eurocode 2: Design of concrete structures. Part 1–1: General rules and rules for buildings*. EN 1992-1-1:2004. Brussels, Belgium: CEN.
- CEN (European Committee for Standardization). 2004b. *Eurocode 2: Design of concrete structures. Part 1–2: General rules—Structural fire design*. EN 1992-1-2:2004. Brussels, Belgium: CEN.
- CEN (European Committee for Standardization). 2005. *Eurocode 4: Design of composite steel and concrete structures. Part 1–2: General rules—Structural fire design*. EN 1994-1-2:2005. Brussels, Belgium: CEN.
- CEN (European Committee for Standardization). 2019. *Eurocode 2: Design of concrete structures. Part 1–2: General—Structural fire design*. prEN 1992-1-2:2019-10. Brussels, Belgium: CEN.
- Colombo, M., M. di Prisco, and R. Felicetti. 2010. “Mechanical properties of steel fibre reinforced concrete exposed at high temperatures.” *Mater. Struct.* 43 (4): 475–491. <https://doi.org/10.1617/s11527-009-9504-0>.
- Diederichs, U., M. C. Alonso, and U.-M. Jumppanen. 2009. “Concerning effects of moisture content and external loading on deterioration of high

- strength concrete exposed to high temperature.” In *Proc., 1st Int. Workshop on Concrete Spalling due to Fire Exposure*, edited by F. Dehn, and E. Koenders, 269–278. Leipzig, Germany: MFPA Institute Leipzig.
- Felicetti, R., and P. G. Gambarova. 1998. “Effects of high temperature on the residual compressive strength of high-strength siliceous concretes.” *ACI Mater. J.* 95 (4): 395–406. <https://doi.org/10.14359/382>.
- Felicetti, R., and P. G. Gambarova. 1999. “On the residual tensile properties of high-performance siliceous concrete exposed to high temperature.” In *Proc., Workshop on ‘Mechanics of Quasi-Brittle Materials and Structures’*, edited by G. Pijaudier-Cabot, Z. Biinar, and B. Gérard, 167–186. Paris: HERMES.
- Felicetti, R., P. G. Gambarova, M. P. N. Sora, and G. A. Khoury. 2000. “Mechanical behaviour of HPC and UHPC in direct tension at high temperature and after cooling.” In *Proc., 5th Symp. on Fibre-Reinforced Concrete BEFIB 2000*, edited by P. Rossi, and G. Chanvillard, 749–758. Cachan, France: RILEM Publications S.A.R.L.
- fib. 1990. *fib bulletin 1: Structural concrete—Textbook on behaviour, design and performance. Updated knowledge of the CEB/FIP model code 1990*. Lausanne, Switzerland: fib.
- fib. 2007. *fib bulletin 38: Fire design of concrete structures—Materials, structures and modelling. State-of-the-art report*. Lausanne, Switzerland: fib.
- fib. 2013. *fib model code for concrete structures 2010*. Berlin: Ernst & Sohn.
- Ghandehari, M., A. Behnood, and M. Khanzadi. 2010. “Residual mechanical properties of high-strength concretes.” *J. Mater. Civ. Eng.* 22 (1): 59–64. [https://doi.org/10.1061/\(ASCE\)0899-1561\(2010\)22:1\(59\)](https://doi.org/10.1061/(ASCE)0899-1561(2010)22:1(59)).
- Hager, I., and K. Mróz. 2019. “Role of polypropylene fibres in concrete spalling risk mitigation in fire and test methods of fibres effectiveness evaluation.” *Materials* 12 (23): 3869. <https://doi.org/10.3390/ma12233869>.
- Hager, I., and P. Pimienta. 2004. “Mechanical properties of HPC at high temperatures.” In *Proc., Int. Workshop fib Task Group, Fire Design of Concrete Structures: What Now? What Next?*, edited by P. G. Gambarova, R. Felicetti, A. Meda, and P. Riva, 95–100. Brescia, Italy: Starrylink.
- ISO. 2010. *Testing of concrete—Part 10: Determination of static modulus of elasticity in compression*. ISO 1920-10:2010(E). Geneva: ISO.
- Jain, A., A. Kathuria, A. Kumar, Y. Verma, and K. Murari. 2013. “Combined use of non-destructive tests for assessment of strength of concrete in structure.” *Procedia Eng.* 54: 241–251. <https://doi.org/10.1016/j.proeng.2013.03.022>.
- Janotka, I., and L. Bágel. 2002. “Pore structures, permeabilities, and compressive strengths of concrete at temperatures up to 800°C.” *ACI Mater. J.* 99 (2): 196–200. <https://doi.org/10.14359/11713>.
- Kalifa, P., G. Chéné, and C. Gallé. 2001. “High-temperature behaviour of HPC with polypropylene fibres—From spalling to microstructure.” *Cem. Concr. Res.* 31 (10): 1487–1499. [https://doi.org/10.1016/S0008-8846\(01\)00596-8](https://doi.org/10.1016/S0008-8846(01)00596-8).
- Khalik, W., and V. Kodur. 2012. “High temperature mechanical properties of high-strength fly ash concrete with and without fibers.” *ACI Mater. J.* 109 (6): 665–674. <https://doi.org/10.14359/51684164>.
- Khoury, G. A. 1992. “Compressive strength of concrete at high temperatures: A reassessment.” *Mag. Concr. Res.* 44 (161): 291–309. <https://doi.org/10.1680/mac.1992.44.161.291>.
- Khoury, G. A., S. Algar, R. Felicetti, and P. G. Gambarova. 1999. “Mechanical behaviour of HPC and UHPC concretes at high temperatures in compression and tension.” In *Proc., ACI Int. Conf. on ‘State-of-the-Art in High Performance Concrete’*. Farmington Hills, MI: American Concrete Institute.
- Kim, J. J., and M. Reda Taha. 2014. “Experimental and numerical evaluation of direct tension test for cylindrical concrete specimens.” *Adv. Civ. Eng.* 2014: 156926. <https://doi.org/10.1155/2014/156926>.
- Kodur, V. 2014. “Properties of concrete at elevated temperatures.” *Int. Scholarly Res. Not.* 2014: 468510. <https://doi.org/10.1155/2014/468510>.
- Lam, E. S. S., and S. Fang. 2014. “Direct tensile behavior of normal-strength concrete at elevated temperatures.” *ACI Mater. J.* 111 (6): 641–649. <https://doi.org/10.14359/51686915>.
- Lemaitre, J., and J. L. Chaboche. 1990. *Mechanics of solid materials*. Cambridge, UK: Cambridge University Press.
- Matysík, M., L. Carbol, Z. Chobola, R. Dvořák, and I. Plšková. 2018. “Comparison of ultrasonic methods for thermally damaged concrete nondestructive testing.” *Key Eng. Mater.* 776: 86–91. <https://doi.org/10.4028/www.scientific.net/kem.776.86>.
- Mechtcherine, V., H. Garrecht, and H. K. Hilsdorf. 1995. “Effect of temperature and loading rate on fracture behaviour of concrete subjected to uniaxial tension.” In *Proc., 2nd Int. Conf. on Fracture Mechanics of Concrete Structures*, edited by F. H. Wittmann, 719–728. Freiburg, Germany: Aedificatio.
- Morita, T., H. Saito, and H. Kumagai. 1992. “Residual mechanical properties of high-strength concrete members exposed to high temperature. Part 1: Test on material properties.” In *Proc., Summaries of Technical Papers of Annual Meeting*. Niigata, Japan: Architectural Institute of Japan.
- Nakamura, H., and T. Higai. 2001. “Compressive fracture energy and fracture zone length of concrete.” In *Modeling of inelastic behavior of RC structures under seismic loads*, edited by P. B. Shing and T.-A. Tanabe, 471–487. Reston, VA: ASCE.
- Naus, D. J. 2006. “A review of the effects of elevated temperature on concrete materials and structures.” *Proc., Int. Conf. on Nuclear Engineering*. Rockville, MD: Nuclear Regulatory Commission.
- Nechnech, W., F. Meftah, and J. M. Reynouard. 2002. “An elasto-plastic damage model for plain concrete subjected to high temperatures.” *Eng. Struct.* 24 (5): 597–611. [https://doi.org/10.1016/S0141-0296\(01\)00125-0](https://doi.org/10.1016/S0141-0296(01)00125-0).
- Neuenschwander, M., M. Knobloch, and M. Fontana. 2016. “Suitability of the damage-plasticity modelling concept for concrete at elevated temperatures: Experimental validation with uniaxial cyclic compression tests.” *Cem. Concr. Res.* 79 (Jan): 57–75. <https://doi.org/10.1016/j.cemconres.2015.07.013>.
- Niry Razafinjato, R., A. L. Beaucour, R. L. Hebert, B. Ledesert, R. Bodet, and A. Noumowe. 2016. “High temperature behaviour of a wide petrographic range of siliceous and calcareous aggregates for concretes.” *Constr. Build. Mater.* 123 (Oct): 261–273. <https://doi.org/10.1016/j.conbuildmat.2016.06.097>.
- Noumowe, A. 2003. “Temperature distribution and mechanical properties of high-strength silica fume concrete at temperatures up to 200°C.” *ACI Mater. J.* 100 (4): 326–330. <https://doi.org/10.14359/12671>.
- Noumowe, A. 2005. “Mechanical properties and microstructure of high strength concrete containing polypropylene fibres exposed to temperatures up to 200°C.” *Cem. Concr. Res.* 35 (11): 2192–2198. <https://doi.org/10.1016/j.cemconres.2005.03.007>.
- Noumowe, A., P. Clastres, G. Debicki, and J. L. Costaz. 1996. “Transient heating effect on high strength concrete.” *Nucl. Eng. Des.* 166 (1): 99–108. [https://doi.org/10.1016/0029-5493\(96\)01235-6](https://doi.org/10.1016/0029-5493(96)01235-6).
- Osmolska, M. J., T. Kanstad, M. A. N. Hendriks, K. Hornbostel, and G. Markeset. 2019. “Durability of pretensioned concrete girders in coastal climate bridges: Basis for better maintenance and future design.” *Struct. Concr.* 20 (6): 2256–2271. <https://doi.org/10.1002/suco.201900144>.
- Phan, L. T., and N. J. Carino. 2001. *Mechanical properties of high-strength concrete at elevated temperatures*. NIST Interagency/Internal Rep. No. (NISTIR)-6726. Gaithersburg, MD: NIST.
- Phillips, D. V., and Z. Binsheng. 1993. “Direct tension tests on notched and un-notched plain concrete specimens.” *Mag. Concr. Res.* 45 (162): 25–35. <https://doi.org/10.1680/mac.1993.45.162.25>.
- Pimienta, P., J.-C. Mindeguia, G. Debicki, U. Diederichs, I. Hager, S. Huismann, U.-M. Jumppanen, F. Meftah, K. Mróz, and K. Pistol. 2019. “Mechanical properties.” In *Physical properties and behaviour of high-performance concrete at high temperature: State-of-the-art report of the RILEM technical committee 227-HPB*, edited by P. Pimienta, R. J. McNamee, and J.-C. Mindeguia, 71–218. Cham, Switzerland: Springer.
- Poon, C. S., S. Azhar, M. Anson, and Y. L. Wong. 2001. “Comparison of the strength and durability performance of normal- and high-strength pozzolanic concretes at elevated temperatures.” *Cem. Concr. Res.* 31 (9): 1291–1300. [https://doi.org/10.1016/S0008-8846\(01\)00580-4](https://doi.org/10.1016/S0008-8846(01)00580-4).
- Robert, F., and H. Colina. 2009. “The influence of aggregates on the mechanical characteristics of concrete exposed to fire.” *Mag. Concr. Res.* 61 (5): 311–321. <https://doi.org/10.1680/mac.2007.00121>.

- Rossi, P., J. G. M. van Mier, F. Toutlemonde, F. Le Maou, and C. Boulay. 1994. "Effect of loading rate on the strength of concrete subjected to uniaxial tension." *Mater. Struct.* 27 (5): 260–264. <https://doi.org/10.1007/BF02473042>.
- Sancak, E., Y. D. Sari, and O. Simsek. 2008. "Effects of elevated temperature on compressive strength and weight loss of the light-weight concrete with silica fume and superplasticizer." *Cem. Concr. Compos.* 30 (8): 715–721. <https://doi.org/10.1016/j.cemconcomp.2008.01.004>.
- Sargin, M., and V. K. Handa. 1969. *A general formulation for the stress-strain properties of concrete*. Waterloo, ON: Univ. of Waterloo.
- Schneider, U., ed. 1985. *RILEM-committee 44-PHT: Behaviour of concrete at high temperatures*. Kassel, Germany: Dept. of Civil Engineering, Gesamthochschule, Kassel Univ.
- Schneider, U., et al. 2000. "RILEM TC 129-MHT: Test methods for mechanical properties of concrete at high temperatures. Part 4: Tensile strength for service and accident conditions." *Mater. Struct.* 33 (228): 219–223. <https://doi.org/10.1007/BF02479330>.
- Schneider, U., et al. 2004. "RILEM TC 129-MHT: Test methods for mechanical properties of concrete at high temperatures. Part 5: Modulus of elasticity for service and accident conditions." *Mater. Struct.* 37 (2): 139–144. <https://doi.org/10.1007/BF02486610>.
- Schneider, U., et al. 2007. "RILEM TC 200-HTC: Mechanical concrete properties at high temperatures—Modelling and applications. Part 2: Stress-strain relation." *Mater. Struct.* 40 (9): 855–864. <https://doi.org/10.1617/s11527-007-9286-1>.
- Shah, S. N. R., F. W. Akashah, and P. Shafiqh. 2019. "Performance of high strength concrete subjected to elevated temperatures: A review." *Fire Technol.* 55 (5): 1571–1597. <https://doi.org/10.1007/s10694-018-0791-2>.
- Siddique, R., and A. N. Noumowe. 2010. "An overview of the properties of high-strength concrete subjected to elevated temperatures." *Indoor Built Environ.* 19 (6): 612–622. <https://doi.org/10.1177/1420326X09346228>.
- Sullivan, P. J. E., and R. Sharshar. 1992. "The performance of concrete at elevated temperatures (as measured by the reduction in compressive strength)." *Fire Technol.* 28 (3): 240–250. <https://doi.org/10.1007/BF01857693>.
- Tanyildizi, H. 2009. "Fuzzy logic model for prediction of mechanical properties of lightweight concrete exposed to high temperature." *Mater. Des.* 30 (6): 2205–2210. <https://doi.org/10.1016/j.matdes.2008.08.030>.
- Thelandersson, S. 1974. *Mechanical behaviour of concrete under torsional loading at transient, high-temperature conditions*. Lund, Sweden: Univ. of Lund.
- van Vliet, M. R. A., and J. G. M. van Mier. 1996. "Experimental investigation of concrete fracture under uniaxial compression." *Mech. Cohesive-Frictional Mater.* 1 (1): 115–127. [https://doi.org/10.1002/\(SICI\)1099-1484\(199601\)1:1<115::AID-CFM6>3.0.CO;2-U](https://doi.org/10.1002/(SICI)1099-1484(199601)1:1<115::AID-CFM6>3.0.CO;2-U).
- van Vliet, M. R. A., and J. G. M. van Mier. 1999. "Effect of strain gradients on the size effect of concrete in uniaxial tension." In Vol. 95 of *Fracture scaling*, 195–219. Dordrecht, Netherlands: Springer.
- Varona, F. B., F. J. Baeza, D. Bru, and S. Ivorra. 2018. "Influence of high temperature on the mechanical properties of hybrid fibre reinforced normal and high strength concrete." *Constr. Build. Mater.* 159 (Jan): 73–82. <https://doi.org/10.1016/j.conbuildmat.2017.10.129>.
- Xing, Z., A. L. Beaucour, R. L. Hebert, A. Noumowe, and B. Ledesert. 2011. "Influence of the nature of aggregates on the behaviour of concrete subjected to elevated temperature." *Cem. Concr. Res.* 41 (4): 392–402. <https://doi.org/10.1016/j.cemconres.2011.01.005>.
- Xing, Z., R. L. Hebert, A. L. Beaucour, B. Ledesert, and A. Noumowe. 2014. "Influence of chemical and mineralogical composition of concrete aggregates on their behaviour at elevated temperature." *Mater. Struct.* 47 (11): 1921–1940. <https://doi.org/10.1617/s11527-013-0161-y>.
- Zheng, W., A. K. H. Kwan, and P. K. K. Lee. 2001. "Direct tension test of concrete." *ACI Mater. J.* 98 (1): 63–71. <https://doi.org/10.14359/10162>.
- Zhen-Hai, G., and Z. Xiu-Qin. 1987. "Investigation of complete stress-deformation curves for concrete in tension." *ACI Mater. J.* 84 (4): 278–285. <https://doi.org/10.14359/1616>.